Aeroacoustic Investigation of a Generic Rotor Model Using a Hybrid Finite-Volume, Finite-Element Computational Scheme with Sliding Mesh Interfaces

Clemens Junger[1], Andreas Hüppe[1], Manfred Kaltenbacher[1]

[1] *Vienna University of Technology, 1040 Wien, Austria, Email: clemens.junger@tuwien.ac.at*

Abstract

Computing the flow induced sound in rotating systems such as in ventilators and compressors yields additional challenges compared to setups without moving parts. In our contribution we apply a newly developed, hybrid computational scheme to a two-dimensional geometry, consisting of two infinitely long cylinders rotating around a common axis in a quiescent medium. The dominant sound producing phenomenon in this setup is the vortex shedding at the individual cylinders as well as the interaction between them.

The flow is computed by solving the incompressible Navier- Stokes (NS) equations using the open source software OpenFOAM, which provides the Arbitrary Mesh Interface (AMI) to handle rotating systems. Due to an energy conserving interpolation scheme, it is possible to use a much coarser computational grid for the acoustic calculation to increase computational efficiency. The propagating sound is computed by solving the acoustic wave equation by the Finite-Element (FE) solver CFS++, which uses a Nitsche type mortaring to couple rotating and stationary mesh. To account for the free radiation condition at the domain boundary, the perfectly matched layer (PML) technique is applied.

Introduction

Sound generated by rotating systems range from helicopters over compressors to fans. Numerical simulations can help to understand the sound producing mechanisms but the computation yields additional challanges for rotating systems [1]. To take into account moving parts in a volume discretization scheme, the domain is decomposed in a rotating and a steady region sharing a common interface. A main problem with rotating grids is the grid interface. There should be neither non-physical energy loss over the interface nor refraction and reflection in the computed flow and acoustic fields. Hence special treatments for the interface between rotating and nonrotating grids are needed [4].

In the following, we briefly introduce Lighthill's aeroacoustic analogy and their utilization in the method of Ffowcs-Williams and Hawkings (FWH) which is commonly applied for sound generation by moving obstacles. The FWH method requires a Green's function to describe the wave propagation, which limitates its applicability. To overcome this, we utilize a volume discrtization approach based on the finite element method to solve for the acoustic wave propagation in arbitrary domains.

Aeroacoustic Analogy

The bases of the following part are the Navier-Stokes equations that describe the flow of a Newtonian fluid. They are well known as the conservation equation of mass

$$\frac{\partial \rho}{\partial t} + \nabla \cdot (\rho \mathbf{u}) = 0 \tag{1}$$

and the conservation of momentum

$$\rho \frac{\partial \mathbf{u}}{\partial t} + (\rho \mathbf{u} \cdot \nabla)\mathbf{u} = -\nabla p + \nabla \boldsymbol{\tau} \tag{2}$$

with the density ρ, the velocity $\mathbf{u}$, the pressure p and the viscous stress tensor $\boldsymbol{\tau}$.

The hybrid aeroacoustic approach was first introduced by Lighthill [6] who described an analogy for free stream sound. By combining the momentum conservation equations in Reynolds form and the mass conservation equation he derived a wave equation for the fluctuation of the density $\rho' = \rho - \rho_0$ with a constant speed of sound c_0 and the second spacial derivative of the Lighthill tensor $\mathbf{T}$ as a source term.

$$\left(\frac{1}{c_0^2}\frac{\partial^2}{\partial t^2} - \Delta\right)(c_0^2(\rho - \rho_0)) = \Delta \mathbf{T} \ . \tag{3}$$

The Lighthill tensor is defined as

$$\mathbf{T} = \rho(\mathbf{u} \otimes \mathbf{u}) + ((p - p_0) - c_0^2(\rho - \rho_0))\mathbf{I} - \boldsymbol{\tau} \tag{4}$$

with $p' = p - p_0$ the pressure fluctuaction and $\mathbf{I}$ the unitiy tensor. The left hand side describes the wave propagation and the right hand side describes the acoustic source terms. With known $\mathbf{T}$, e.g. as a result of a CFD-calculation, the wave equation can be solved. For any observation point $\mathbf{x}$, the fluctuating density computes by

$$c_0^2(\rho - \rho_0)(\mathbf{x}, t) = \frac{1}{4\pi}\Delta \int_{-\infty}^{\infty} \frac{\mathbf{T}(\mathbf{y}, t - |\mathbf{x} - \mathbf{y}|/c_0)}{|\mathbf{x} - \mathbf{y}|} dy \ . \tag{5}$$

The problem is that this formulation is only applicable for observation points outside the flow field and just for free radiation. Furthermore the integral gives just the result in one specific point. If the results are needed in many points the integral has to be solved several times.

Lighthills analogy was improved by Curle and Ffowcs Williams-Hawkings [1] for solid bodies in the flow field. Therefore, in the whole region Ω, a region that surrounds the body Ω_s is described by Γ_s (Fig. 1). The equation is

now given in the formulation

$$\left(\frac{1}{c_0^2}\frac{\partial^2}{\partial t^2} - \Delta\right)(c_0^2(\rho-\rho_0)H(\Gamma_s)) = \Delta\mathbf{T}H(\Gamma_s) - \nabla\left((\rho(\mathbf{u}\otimes\mathbf{u}) + (p-p_0)\mathbf{I} - \boldsymbol{\tau})\nabla H(\Gamma_s)\right) + \frac{\partial}{\partial t}\left(\rho\mathbf{u}\nabla H(\Gamma_s)\right) \ , \quad (6)$$

where $H(\Gamma_s)$ is the heavyside function. This equation looks very similar to (3) but the second and third term on the right hand side are additional source terms that result from the body.

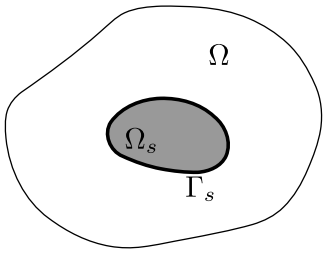

Figure 1: Solid body with volume Ω_s and surface Γ_s in the total domain Ω.

For an incompressible flow without loss terms (1) and (2) reduce to

$$\nabla\cdot\mathbf{u} = 0 \quad (7)$$

and

$$\rho\frac{\partial\mathbf{u}}{\partial t} + \rho(\mathbf{u}\cdot\nabla)\mathbf{u} + \nabla p = 0 \ . \quad (8)$$

These equations are solved with a Finite-Volume (FV) scheme that is mainly used to solve conservation equations. The basic idea of the FV is to approximate the conservation of a physical quantity q

$$\frac{\partial q}{\partial t} + \nabla\cdot\mathbf{f}(q) = 0 \quad (9)$$

in an integral form applying Gauss' integral theorem

$$\frac{d}{dt}\int_\Omega q d\Omega + \int_\Gamma \mathbf{f}(q)\cdot\mathbf{n}d\Gamma = 0 \ . \quad (10)$$

By replacing the integral over the boundary by the sum of the flux over all surfaces of a cell, the semi-discrete formulation is obtained. For the fully discretized formulation also the time has to be discretized. The main difficulty is to approximate the numerical flux over the faces of the cells. For detail we refere to [11].

The main idea of the FE method is to solve a partial differential equation (PDE) in the weak formulation by multiplying (3) with a test function φ

$$\varphi\left(\frac{1}{c_0^2}\frac{\partial^2}{\partial t^2} - \Delta\right)c_0^2\rho' = \varphi\Delta\mathbf{T} \ , \quad (11)$$

integrating over the whole domain and performing integration by parts [7]

$$\int_\Omega \varphi\frac{1}{c_0^2}\frac{\partial^2}{\partial t^2}\rho' d\Omega + \int_\Omega \nabla\varphi\cdot\nabla\rho' d\Omega - \int_\Gamma \varphi\frac{\partial}{\partial\mathbf{n}}\rho' d\Gamma = \int_\Omega \varphi\Delta\mathbf{T}d\Omega \ . \quad (12)$$

With the approximation for a continuous variable by discrete values multiplied with basis functions φ_k

$$\rho' \approx \rho'^h = \sum_{k=1}^{N}\rho'_k\varphi_k \ , \quad (13)$$

we obtain the semi discrete Galerkin formulation. For a constant c_0^2 (12) can also be derived in the pressure formulation.

In our approach we compute the source terms from incompressible CFD simulations. To solve the wave equation, we apply our in house research program CFS++ which is based on an FE method. With this approach it is possible to describe the propagation of sound directly in the flow field. Furthermore, the acoustic region can be larger than the flow region to account for the propagation domain. To prohibit unphysical reflections at the border of the mesh we use the damping method of the perfectly matched layers (PML) [7]. For the investigations in this paper we used the assumption that for low Mach numbers the flow is completely incompressible. Hence the source term can be written as

$$\Delta\mathbf{T} = -\Delta p^{ic} \ . \quad (14)$$

with the incompressible pressure p^{ic}.

Moving Meshes / Nonconforming grids

A main problem with rotating grids is the interface between the moving and the stationary part. To solve (10) the flux over the cell boundary needs a special treatment at the interface. To give a short overview the used algorithms are explained. For detailed description it is referred to [3].

CFD

For the CFD calculation in OpenFOAM, there is a special interface type available which is called the Arbitrary Mesh Interface (AMI). For a curved interface the linear elements on the interface have to be small enough to describe the curvature. On the AMI the data transfer from one surface to another is done by a local Galerkin projection according to [3]. This method of projecting a quantity q from the donor surface with index D to the target surface with index T is based on the minimization of the L_2-Norm of the difference $q_\mathrm{D} - q_\mathrm{T}$. The quantity q is defined discretely with the basis functions φ as $q = \sum_{i=1}^{N} q^{(i)}\varphi^{(i)}$. For a two-dimensional interface the discrete values of φ are shown in Fig. 2. The quantity of the donor region q_D refers to

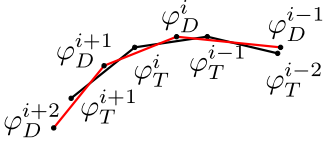

Figure 2: Interpolation of a quantity from a donor face to a target face in 2D.

the quantity in the target region q_T by

$$M_\mathrm{T} q_\mathrm{T} = M_\mathrm{TD} q_\mathrm{D} \ . \tag{15}$$

In (15) the matrices compute as

$$(M_\mathrm{T})_{ij} = \int_\Gamma \varphi_\mathrm{T}^{(i)} \varphi_\mathrm{T}^{(j)} dV, \quad i,j \in \{1, \cdots, N_\mathrm{T}\} \tag{16}$$

$$(M_\mathrm{TD})_{ij} = \int_\Gamma \varphi_\mathrm{T}^{(i)} \varphi_\mathrm{D}^{(j)} dV, \quad i \in \{1, \cdots, N_\mathrm{T}\}, \quad j \in \{1, \cdots, N_\mathrm{D}\} \ . \tag{17}$$

The main challenge is the creation of the matrix M_TD as it contains basis functions of both sides of the interface. The proposed way is to project the basis functions of both areas on a common super-mesh and perform the integration there.

CAA

The method in CFS++ is also based on non-conforming meshes on the surfaces of the interface according to [12] (for the implementation see also [4]). For a grid consisting of two domains, (12) has to be fulfilled for both domains on the common interface Γ_I. Since the normal vectors are orientated in different directions a unique normal vector $\mathbf{n}_I$ is introduced. Setting the right hand side for simplicity to zero, the equations for both domains can be written as

$$\int_{\Omega_1} \varphi_1 \frac{1}{c_0^2} \frac{\partial^2 p_1'}{\partial t^2} d\Omega + \int_{\Omega_1} \nabla \varphi_1 \cdot \nabla p_1' d\Omega - \int_{\Gamma_1} \varphi_1 \frac{\partial p_1'}{\partial \mathbf{n}_I} d\Gamma = 0 \tag{18}$$

and

$$\int_{\Omega_2} \varphi_2 \frac{1}{c_0^2} \frac{\partial^2 p_2'}{\partial t^2} d\Omega + \int_{\Omega_2} \nabla \varphi_2 \cdot \nabla p_2' d\Omega + \int_{\Gamma_2} \varphi_2 \frac{\partial p_2'}{\partial \mathbf{n}_I} d\Gamma = 0 \ . \tag{19}$$

A physical requirement is the equality of the normal derivative of p' at the interface

$$\frac{\partial p_1'}{\partial \mathbf{n}_I} = \frac{\partial p_2'}{\partial \mathbf{n}_I} \ . \tag{20}$$

By adding (18) and (19) and taking into account (20) the integral over Γ_I reads as follows

$$\int_{\Gamma_I} (\varphi_2 - \varphi_1) \frac{\partial p_1'}{\partial \mathbf{n}_I} d\Gamma \ . \tag{21}$$

Equation (21) is asymmetric and therefor an additional term is added to restore the symmetry in the equation system

$$\int_{\Gamma_I} \frac{\partial \varphi_1}{\partial \mathbf{n}_I} (p_1' - p_2') d\Gamma = 0 \ . \tag{22}$$

Furthermore an additional penalty term is added to stablize the numerical scheme containing a constant β, h_E a constant depending on the size of the intersecting elements and E_I the surface of the intersecting elements

$$\beta \sum_{E_I} \frac{1}{h_E} \int_{E_I} (\varphi_1 - \varphi_2)(p_1' - p_2') d\Gamma = 0 \ . \tag{23}$$

This semi discrete formulation can now be written in matrix form

$$M \ddot{\mathbf{p}'} + K \mathbf{p}' = 0 \ . \tag{24}$$

On the rotating part of the mesh, the wave equation has to be modified. The rotation of the grid requires an adaption of the time derivative in the wave equation to prevent refractions of acoustic waves crossing the interface. Hence the substantial derivative is used on the left hand side of the wave equation leading to

$$\frac{D^2}{Dt^2} p' - \Delta p' \tag{25}$$

with the differential operator

$$\frac{D^2}{Dt^2} = \left(\frac{\partial}{\partial t} + \mathbf{u}_\mathrm{rot} \nabla \right)^2 \tag{26}$$

and $\mathbf{u}_\mathrm{rot}$ as the rotating speed on the disc. The spacial derivative of the wave equation is not effected because the grid is just rotating and not deforming.

Application

The setup consists of two infinitely long cylinders rotating around a common axis in a quiescent medium (Fig. 3). The diameter of the cylinders is $d = 2\,\mathrm{mm}$, the radius to the axis is $r = 95\,\mathrm{mm}$ and the rotation velocity of the cylinders $\mathbf{u}_\mathrm{rot} = 20\,\mathrm{m/s}$. The Reynolds number of the cylinders computes to $Re = \mathbf{u}_\mathrm{rot} \cdot d/\nu = 2666.\overline{6}$ and the flow will be considered as laminar. The shaft is modeled in the rotation axis with a radius of 12.5 mm and the interface of the rotating grid has a radius of 150 mm. This setup is used refering to an experimental work with similar setups [5].

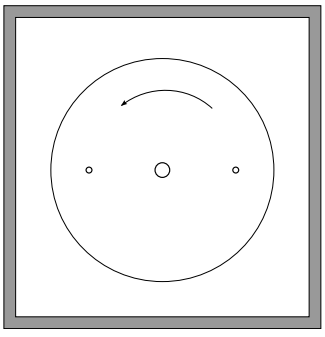

Figure 3: Sketch of the rotating geometry in a square surrounded by a PML.

The cylinders rotate and generate a vortex street behind them but also induce a rotation of the fluid. Due to the movement of the fluid, the relative velocity of the cylinders and thereby the Reynolds number is decreased. The vortices of the wake dissipate but they also interact with

the passing cylinders. Since there is no flow that transports the vortices away, a high number of rotations need to be computed until the flow reaches a steady state and a meanful acoustic computation can be carried out. For the presented compuations, 10 rotations of the cylinders are simulated before the acoustic computation starts.

Under ideal conditions it can be estimated that a steady state is reached when the whole fluid in the region is circulating since there is no counter acting force. To reduce computational effort and with the knowledge that the main source terms are at the cylinder and in its wake, the flow field is considered to be steady state when the flow near the cylinder is not changing anymore. This is evaluated by the fluid forces on the cylinders.

The shedding frequency of the vortex street can be estimated in analogy to a normal cylinder in cross flow [8] with the Strouhal number $St = f \cdot d/\mathbf{u}_{\text{rot}}$ where f is the frequency. For low Reynolds numbers the Strouhal number is approximately 0.2 and a shedding frequency of $f = 2\,\text{kHz}$ can be estimated. Due to the rotation of the flow the relative velocity is supposed to be smaller and the shedding frequency decreases. Furthermore, the vortices of the incoming flow and the different peripheral speed from the inside to the outside of the rotation cylinder lead to a broadening of the main frequency.

The vortex shedding is the main tonal acoustic source. However due to the aerodynamic irregularities a sharp peak cannot be expected. An observer can also see the cylinder passing frequency, which is for this setup with two cylinders at $f = 67\,\text{Hz}$.

For the CFD calculations, the computational mesh with a refinement near the cylinder results in 209000 cells. The used CFD solver of OpenFOAM uses a combination of the PISO and SIMPLE algorithm and is also able to handle dynamic meshes. Because of the low Reynolds number no turbulence model was used. The time step was dynamically adapted according to the Courant-Friedrichs-Lewy number and for the export time step a value of $\Delta t = 2 \cdot 10^{-5}\,\text{s}$ was used. The real time of the calculation was 0.3 s.

The calculation of the source terms from the CFD data is performed directly on the CFD grid by CFS++. The interpolation is performed with the node results in a conservative way [10]. Anyhow, in this work the CAA grid is just slightly coarser than the CFD grid in order to compute acoustic waves up to 5 kHz.

For the CAA calculations a mesh with an uniform cell size in the whole domain and a refinement just around the cylinders with about 95000 elements was used. Beyoned this freqeuncy, the numerical error of the computation increases. The square acoustic domain has a PML region to prevent reflections of outgoing waves.

The different grid spacing is shown for the region of one cylinder in Fig. 4. The black grid is used for CFD, where the red is used for CAA. It can be seen that the CAA has no boundary layers and the grid size increases rapidly. The fine cells in the CAA grid are just needed to resolve the curvature of the cylinder.

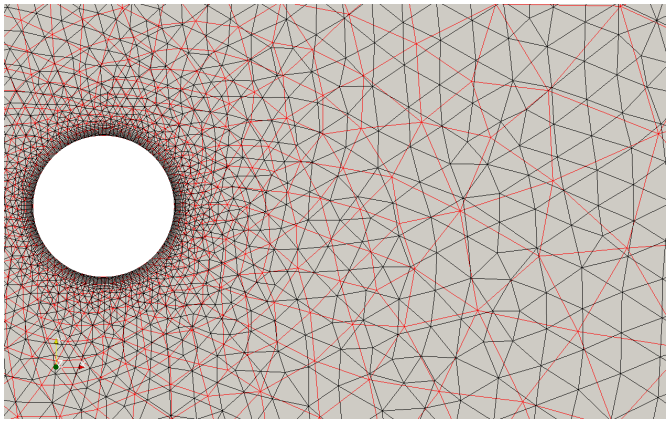

Figure 4: Comparison of CFD mesh (black) and CAA mesh (red) around the cylinder.

Results

The flow field develops as the cylinders rotate through air and the vortex street arises behind the cylinders. Figure 5 shows the pressure field around one cylinder, moving from the left side of the picture to the right. At the right side of the cylinder a constant area of high pressure is seen which results from the stagnation point of the flow. The vortices have a lower pressure in the vortex center as can be seen at the left side of the picture. The vortex shedding is, obviously, a transient phenomenon and the picture shows the shedding of a vortex at the bottom. The flow field is assumed to reach a steady state after ten revolutions. The results of the CFD calculation give an average coefficient of drag of $c_D = 1.14$, which is close to the common value of 1.2 in literature for infinit long cylinders and $Re < 9 \cdot 10^4$.

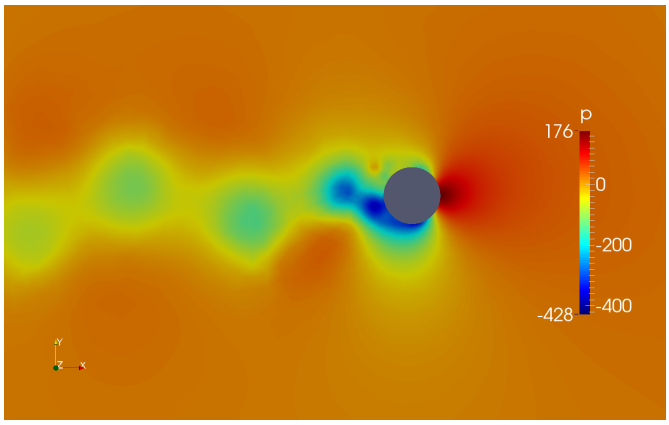

Figure 5: Kinematic pressure distribution around one cylinder due to the vortex street.

After the computation of the source terms the main sound producing frequencies are already detectable in the field. The highest values are at the cylinders and in the wake of them. Figure 6 shows the FFT (Fast Fourier Transformation) of a monitoring point in the wake. A sharp peak

can be seen at the cylinder passing frequency of 67 Hz. Also at 33 Hz and higher harmonics, tonal components are visible, as expected. At about 200 Hz the amplitude of the source term is decreasing until two broad peaks can be seen. The first has it's maximum at about 1800 Hz, which corresponds to the vortex shedding frequency and the second at the double frequency. The double frequency occures, because the vortex sheddings of both sides combine behind the cylinder.

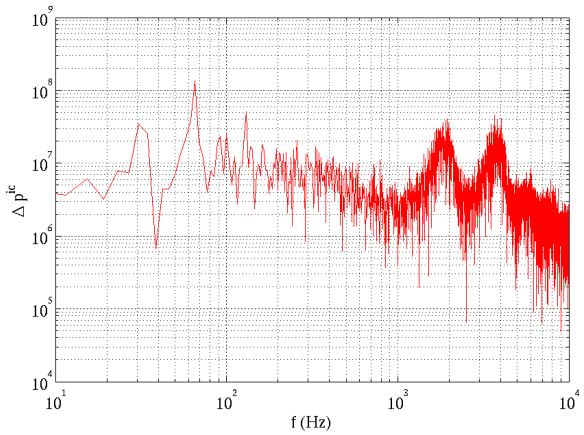

Figure 6: FFT of the source term Δp^{ic} in the wake of a cylinder.

The CAA calculations provides the acoustic fields. In Fig. 7, the fluctuating pressure distribution is displayed. The main acoustic sources are as expected directly at the cylinder and in the vortex street. From there, the waves propagate over the interface through the stationary mesh, to the PML surrounding the domain to absorb the outgoing waves without reflection. Outside the rotating region, larger vortices can be seen in the pressure field that move very slowly. They disturb the sound propagation, but seem to be just minor acoustic sources.

Figure 8 shows the sound pressure level (SPL) at an observation point close to the left boundary outside the original flow region. At the cylinder passing frequency of 67 Hz the spectrum shows a significant peak but compared to the source term the rise in the double frequency cannot be seen at all. At about 300 Hz the SPL rises slowly until a significant peak between 1450 Hz and 2200 Hz, which result from the vortex shedding as it is described in [5]. The rise in the source terms at the double frequency is just slightly visible in the fluctuating pressure far from the source region. Over 5 kHz the noise in the signal increases and the amplitude drops as the spacial resolution of the grid gets worse.

Conclusion

The newly developed scheme was successfully applied to a rotating two-dimensional system. In this configuration the main sound is generated in the rotating part. The tonal components of the sound could already be investited in the spectrum of the acoustic source terms located in the inner region. From there, waves propagate over the interface until it is damped in the PML-region. No significant unphysical influence of the rotating grid interface can be observed in the acoustic or in the flow results. The acoustic results encourage to do further investigations with an improved three-dimensional mesh.

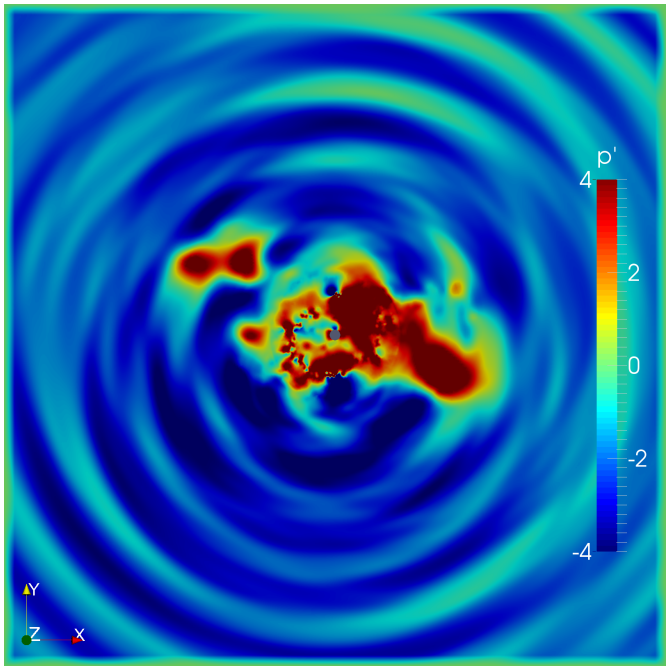

Figure 7: Wave propagation computed with the sourceterm Δp^{ic}.

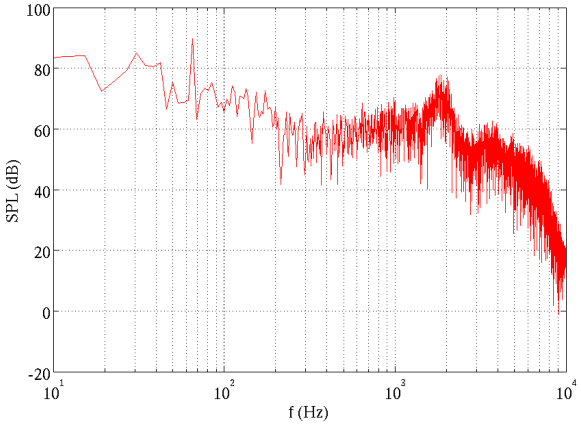

Figure 8: SPL computed with the source term Δp^{ic}.

References

[1] Ffowcs Williams J.E., Hawkings D.L.: **Sound Generation by Turbulence and Surfaces in Arbitrary Motion**, Phil, Transac- tions of the Royal Society, 1969

[2] Nitsche J.A.: **Über ein Variationsprinzip zur Lösung von Dirichlet-Problemen bei Verwendung von Teilräumen, die keinen Randbedingungen unterworfen sind**, Abhandlungen aus dem Mathematischen Seminar der Universität Hamburg, 36, 9–15, 1970/71

[3] Farrell P.E., Maddison J.R.: **Conservative interpolation between volume meshes by local Galerkin projection**, Computer Methods in Applied Mechanics and Engineering (2011)

[4] Hüppe A., Grabinger J., Kaltenbacher M., Reppenhagen A., Dutzler G., Kühnel. W.: **A Non-Conforming Finite Element Method for Computational Aeroacoustics in Rotating Systems**. In Proceedings of the 20th AIAA/CEAS Aeroacoustics Conference, AIAA-2014, 2014. 16-20 June 2014, Atlanta, USA. CD-ROM Proceedings.

[5] Stuber B.: **Untersuchung aerodynamisch erzeugter Schallfelder mit Hilfe der Modellmethode**, Dissertation, TU München, 1967

[6] Lighthill M.J.: **On Sound Generated Aerodynamically. I. General Theory**. Proceedings of the Royal Society of London, 1952

[7] Kaltenbacher B., Kaltenbacher M., Sim I.: **A modied and stable version of a perfectly matched layer technique for the 3-d second order wave equation in time domain with an application to aeroacoustics**, Journal of Computational Physics, 235 (2013), 16 S.

[8] Breuer, M.: **Direkte Numerische Simulation und Large-Eddy Simulation turbulenter Strömungen auf Hochleistungsrechnern**, Shaker Verlag, Aachen, 2002

[9] Escobar, M.:**Finite Element Simulation of Flow-Induced Noise using Lighthill's Acoustic Analogy**, Dissertation, Universität Erlangen-Nürnberg, 2007

[10] Triebenbacher, S.: **Nonmatching Grids dor the Numerical Simulation of Problems from Aeroacoustics and Vibroacoustics**, Dissertation, Alpen-Adria-Universität Klagenfurt, 2011

[11] Ferzinger, J.H., Peric,M,: textbfNumerische Strömungsmechanik, Springer-Verlag, Berlin Heidelberg, 2008

[12] Hansbo A., Hansbo P., Larson M. G.: **A Finite Element Method on Composite Grids based on Nitsche's Method ESAIM**, Math. Model. Num. Anal., 2003